# LARGE SCALE STRUCTURES IN AN ADVERSE PRESSURE GRADIENT TURBULENT BOUNDARY LAYER

*Z. Harun , V. Kulandaivelu, B. Nugroho, M. Khashehchi, J.P. Monty, I. Marusic*

*University of Melbourne, Victoria 3010 , AUSTRALIA.*

**z.harun@pgrad.unimelb.edu.au**

## Abstract

Understanding the structure of wall turbulence is critical to further progress in controlling and predicting the phenomenon. Research now points to the existence of highly organized large-scale structures within turbulent flows. Recently there has been significant development in understanding these large scale structures both through experimental measurement and computations. However, most progress towards understanding the large scale features of wall-bounded shear flow has been in Zero Pressure Gradient (ZPG) turbulent boundary layers (TBL), leaving scope for further research in Adverse and Favourable Pressure Gradients, (A/FPG). The present work is inspired by the recent studies of large scales influences in near-wall turbulence by Hutchins & Marusic (2007) who found that long and meandering features exist throughout the flow. These features appear to be highly energetic with length of O(20$\delta$). This investigation seeks further information about structures in pressure gradient flows through analysis of streamwise velocity statistics and energy spectra. Through a comparison of ZPG and APG flows at matched Kármán number $\delta U_\tau/\nu$, the similarities and differences of these flows will be analyzed structurally.

## 1 Introduction

There are a number of studies in APG flows and some important features have been published and found to share a similar trend. In general, as the strength in APG is increased, a large wake region is observed and broadband turbulent intensities $\overline{u^2}/U_\tau^2$ increase especially in the log and wake region. The non-dimensionalised pressure gradient parameter is defined as $\beta = \frac{\delta^*}{\tau_o}\frac{dP}{dx}$, is used throughout this paper. There are many distinguishing features in APG compared to ZPG and FPG, such as the constants $\kappa$ and $A$ in equation $U^+ = \frac{1}{\kappa}\log(\frac{yU_\tau}{\nu}) + A$ discussed in Nagib and Chauhan (2008). Lee and Sung (2009) found that that the near wall 'streaks' are weakened and the spanwise spacing is 400 viscous wall units in APG flow with $\beta$=1.68. Streaks are defined by Kline et al (1967) as well-organized spatially and temporally dependent motions within the 'laminar sub-layer', lead to the formation of low-speed streaks in the region very near the wall. The streak spacing in ZPG has been known to be 100 viscous wall units. In a comparison study of turbulent pipe, channel and boundary layer flows, Monty et al (2009) pointed out that there is a remarkable difference between the length of the longest energetic structure in the external and internal flows as the distance from the wall increases. Of the many mysteries in this flow, we would like to find the effect of APG on vortical structure using energy spectra study in as accurate a measuring-environment as possible and in relatively high Reynolds number.

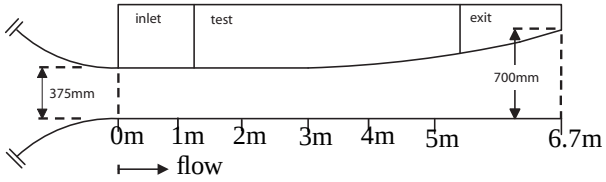


Figure 1: Wind tunnel general geometries

### Facility

The experiments were performed in an open-return blower wind tunnel. The important features of the tunnel are a settling chamber containing honeycomb and five screens followed by a contraction with area ratio of 8.9:1 which leads into an initial inlet section area of 940mm wide by 375mm. The test section's roof, made from acrylic, makes the heights adjustable, it has a length of 4.2m. The sections heights are 375mm at the trip wire (x=0m), 400mm at x=3m and 550mm at x=5m. The geometry is shown in figure 1. This is the same wind tunnel that had been used by previous researchers such as Marusic and Perry (1995) and Jones et al (2001) in their studies of the structure of Z/APG TBL and evolution and structure of sink flow TBL respectively. A number of researchers who performed experiments at constant $\beta$ have reported difficulties setting pressure gradient for the required $\beta$. In our experiment, the linear increment in $C_p$ requires the roof gradient to increase slightly exponentially. We chose a mild gradient because fierce gradient might produce near separation conditions, making accurate measurement difficult (Clauser, 1954).

The wind tunnel is divided into 4 sections, the inlet, the ZPG, APG and outlet sections. Modifications

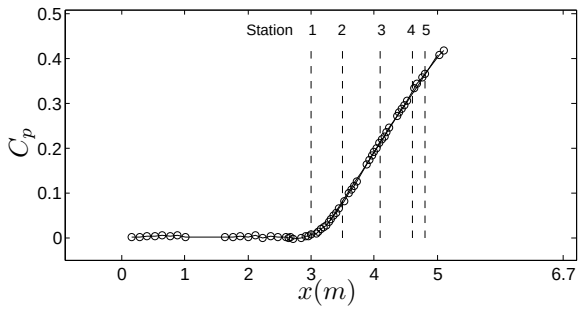


Figure 2: Coefficient of pressure $C_p$

have been made to the wind tunnel roof to get smooth pressure gradients. The pressure gradient was carefully adjusted so that coefficient of pressure defined in equation 1 was set to be within $\pm 1\%$ throughout the velocities tested. Here $P$ is the static pressure measured by the wall tappings, $P_t$ is the reference total pressure, $P_0$ is the reference static pressure and $U_\infty$ is the free-stream velocity. Figure 2 shows $C_p$ plotted against streamwise position (m). The first 10 pressure taps are in the inlet section. The figure shows that the next 15 pressure taps were in ZPG. This is to ensure that the flow was stable before any pressure gradient is introduced.

$$C_p = \frac{p - p_0}{p_t - p_0} = \frac{p - p_0}{\frac{1}{2}\rho {U_\infty}^2} = 1 - \left(\frac{U}{U_\infty}\right)^2 \qquad (1)$$

**Experimental parameters**

All of the measurements were performed using single hot-wire anemometry. The hot-wire probes were all operated in constant temperature mode using an AA Lab Systems AN-1003 anemometer with overheat ratio of 1.8 and the system had a frequency response of at least 50kHz to a 2kHz internal pulse. A Dantec probe support (55H20) was used. Wollaston wires of diameter $\phi = 2.5\mu m$ are soldered to the prong tips and etched to give a platinum filament of the desired length, $l$. When comparisons are made with published data, $\phi = 3.8\mu m$ was used so that almost-exact experimental condition could be made. The length-to-diameter ratio of hot-wire sensors should exceed 200 ($l/d > 200$) in order to minimize attenuation caused by end conduction effects (Ligrani and Bradshaw (1987)). Hutchins et al (2009) confirmed this, thus we have maintained that $l/d > 200$ throughout the experiment.

Since the experiment required measurement at different Kármán numbers, the dimensionless wire length $l^+$ would change as $l^+$ is proportional to $U_\tau$ if the exposed wire length $l$ was maintained. $l^+$ should be as small as possible to reduce spatial resolution problems. Based on the existing data by Hutchins et al (2009), we have chosen $l^+$=16 $\pm$ 1, and for comparison with other published data, we tried to match our $l^+$ with that of the existing data to ensure that scatter due spatial resolutions issues are minimized. In table 1, $U_\infty$ is the free-stream velocity, $U_\tau$ is the friction velocity determined from Clauser chart fit to the logarithmic portion of the mean velocity data (using constants $\kappa$=0.41 and $A = 5.0$) and by Oil Film Interferometry (OFI), they are found to agree very well. The OFI method is described in Chauhan et al (under consideration). Superscript + is used to denote viscous scaling e.g. $z^+ = zU_\tau/\nu$, $U^+ = U/U_\tau$, $t^+ = tU_\tau{}^2/\nu$. The Reynolds number, $Re_\tau$ (Kármán number) is given by $\delta U_\tau/\nu$, where $\delta$ is the boundary layer thickness determined from a modified Coles law of the wall/wake fit to the mean velocity profile in the method shown in detail by Jones et al (2001). $t^+ = tU_\tau{}^2/\nu$ is the non-dimensionalised sample interval, where $t = 1/f_s$, $f_s$ is sampling rate. All experimental parameters are shown in table 1.

The sampling time or total length in seconds of the velocity sample at each height is given by T. This is non-dimensionalised in outer scaling to give boundary layer turn-over times $TU_\infty/\delta$ needs to be large. The largest structure in boundary layers can exceed $20\delta$. Since we are experimenting with flows at APG where sometimes $\beta$ can be very large, we had to keep our boundary layer turnover times $\geq$ 20000 in most of the data.

## 2 Results

**Velocity and broadband turbulent intensity profiles**

Figure 3(a) shows the mean velocity profiles for experiments performed at a matched $Re_\tau$ $\approx$1800. This measurement is possible by moving from one station to the other and a unique velocity is expected for a matched $Re_\tau$. By doing so, $\beta$ is varied and in this case it is from 0 (ZPG flow) until 5.1. The near-wall region shows a good collapse for mean velocity profiles for ZPG and all APG cases in the sense that there is no obvious deviation from $U^+ = y^+$.

It is of great interest to get accurate data in the region near to the wall, 5$<$ $z^+$ $<$20 to provide information about the near-wall structure. Hutchins et al (2009) pointed out that the scatter in viscous-scaled broadband intensity in the near wall region is due in large part to the competing effect of Reynolds number and non-dimensionalised exposed wire length $l^+$: as $Re_\tau$ is increased, large scales structure in the near wall is increased resulting in net increase in $\overline{u^2}/U_\tau^2$. As $l^+$ is increased, the small-scaled fluctuations becomes increasingly attenuated, thus causing net decrease in $\overline{u^2}/U_\tau^2$. For this reason, we paid great attention to spatial resolution issues as our $l^+$ is matched. Figure 3(b) shows the broadband turbulent intensity profiles performed at a matched $Re_\tau$ $\approx$1800. Profiles with least $\overline{u^2}/U_\tau^2$ is the ZPG case. The inner peak magnitude in $\overline{u^2}/U_\tau^2$ is $\approx$ 8. This data lies in good agreement with the $Re_\tau$ effects and $l^+$ resolution studies by Hutchins

| Symbol | $U_\infty$ m/s | $x$ m | $Re_\tau$ | $\delta$ m | $\delta^*$ | $\theta$ | $\Pi$ | $\beta$ | $P^+$ x1$^{-3}$ | $\nu/U_\tau$ $\mu m$ | $d$ $\mu m$ | $l^+$ | $t^+$ | $TU_\infty/\delta$ |
|---|---|---|---|---|---|---|---|---|---|---|---|---|---|---|
| ▽¶ | 11.97 | 5.0 | 2820 | 0.098 | 0.0126 | 0.0095 | 0.59 | ZPG | ZPG | 35.0 | 3.8 | 22 | 0.53 | 14600 |
| ♦! | 16.39 | 4.6 | 2890 | 0.093 | 0.0193 | 0.0129 | 2.04 | 3.83 | 3.57 | 32.0 | 3.8 | 24 | 0.296 | 21243 |
| ▷ ‡ | 14.24 | 3.0 | 1820 | 0.052 | 0.0074 | 0.0055 | 0.65 | ZPG | ZPG | 28.7 | 2.5 | 17 | 0.37 | 21800 |
| ◇ ‡ | 12.70 | 3.5 | 1870 | 0.061 | 0.0095 | 0.0068 | 0.87 | 0.87 | 30.1 | 32.6 | 2.5 | 15 | 0.28 | 31000 |
| o ‡ | 11.40 | 4.1 | 1860 | 0.078 | 0.0142 | 0.0098 | 1.32 | 1.89 | 56.5 | 42.0 | 2.5 | 16 | 0.18 | 21900 |
| □ ‡ | 10.07 | 4.6 | 1850 | 0.093 | 0.0195 | 0.0128 | 1.91 | 3.32 | 88.5 | 50.3 | 2.5 | 16 | 0.12 | 18400 |
| ∗ ‡ | 9.80 | 4.8 | 1880 | 0.104 | 0.0241 | 0.0152 | 2.47 | 5.10 | 119.6 | 55.5 | 2.5 | 15 | 0.10 | 22500 |

Table 1: Experimental parameters for hotwire experiments. All data from the University of Melbourne. ¶ HRNBLWT,! matched HRNBLWT (High Reynolds Number Boundary Layer Wind Tunnel) data, ‡ matched $Re_\tau$ data

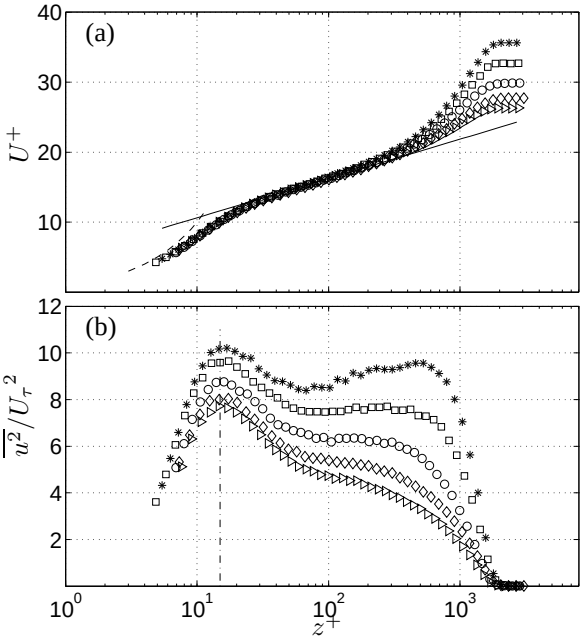


Figure 3: APG flows at matched $Re_\tau \approx 1800$ (a) Mean velocity profiles (b) Broadband turbulent intensity profiles. (▷) $\beta$=0, ZPG case, (◇) $\beta$=0.87, (o) $\beta$=1.89, (□) $\beta$=3.32, (∗) $\beta$=5.10. Solid line shows $U^+ = \frac{1}{\kappa}\ln(z^+) + A$, $\kappa$=0.41 and $A$=5.1, dashed line shows $U^+ = z^+$ and dashed-dot line $z^+$=15.

et al (2009). Moving on towards higher $\beta$, $\overline{u^2}/U_\tau^2$ increases to ≈10 at $\beta$=5.1. This data shows that at a constant Kármán number, $\overline{u^2}/U_\tau^2$ increases as $\beta$ is increased in the inner peak region. Inner peak region occurs at $z^+$=15 for all of the matched $Re_\tau$ data.

**Energy spectra**

All representations of pre-multiplied energy spectra $k_x\phi_{uu}$ are plotted against streamwise wavelength $\lambda_x = 2\pi/k_x$, where wave-number $k_x = 2\pi f/U_c$, $f$ is the frequency and $U_c$ is the convection velocity. This representation is an image of conventional $k_x\phi_{uu}{}^+$ versus $\log(k_x\delta)$ plot and the equal area under the curve represents equal contribution to energy. In ZPG flow, there is a highly energetic peak in the near wall region occurring at $z^+$ ≈15 and $\lambda_x{}^+$ ≈1000 called the 'inner peak'. The 'inner peak' is due to the inner cycle of streaks and quasi-streamwise vortices. The energy shifts to larger wavelength with increased distance from the wall. Hutchins and Marusic (2007b) showed that there is a second peak in the boundary layer spectra map at $z^+ \approx 0.06\delta$ corresponding to superstructures of wavelength $\lambda_x \approx 6\delta$.

We begin our analysis of energy spectra by comparing our data in APG with $\beta$=3.83 and HRNBLWT (ZPG) published in Hutchins et al (2009) with a matched $Re_\tau \approx 2800$. The mean velocity profiles and $\overline{u^2}/U_\tau^2$ are shown in figure 4(a) and (b). The main feature to note between the ZPG and APG flows is that they have similar mean velocity, $U^+$ in the near-wall region towards log region and $U^+$ starts shifting up only approximately in the the wake region. However they have very different $\overline{u^2}/U_\tau^2$ throughout the boundary layer. We must emphasize that $l^+$ is constant throughout the data in regards to the fact that $l^+$ plays a big role in $\overline{u^2}/U_\tau^2$. Broadband turbulent intensities increases from $\overline{u^2}/U_\tau^2 \approx 8$ to ≈ 10 from ZPG to APG in the near-wall region. The shear stress for the APG flow maintains its strength throughout the flow until the wake region. $\overline{u^2}/U_\tau^2$ for ZPG decreases gradually all the way towards the wake region, however, for the APG flow, the strength reduces only slightly towards the logarithmic region and maintains the strength in the wake region before abruptly losing all energy towards the edge of the boundary layer. Overall, the turbulence intensity is higher for APG than ZPG. The $\overline{u^2}/U_\tau^2$ plot shows that turbulence in APG with $\beta$=3.83 and $Re_\tau$=2800 is very strong from the near-wall until the edge of the boundary layer in comparison with the ZPG flow.

We perform a Fourier analysis of the data to investigate in which scales the energy differences occur between the two flows. Results are shown in figure 5(a) & (b). The near-wall energy peak still occurs at the same wave length i.e. $\lambda_x^+ = 1000$, albeit at a relatively

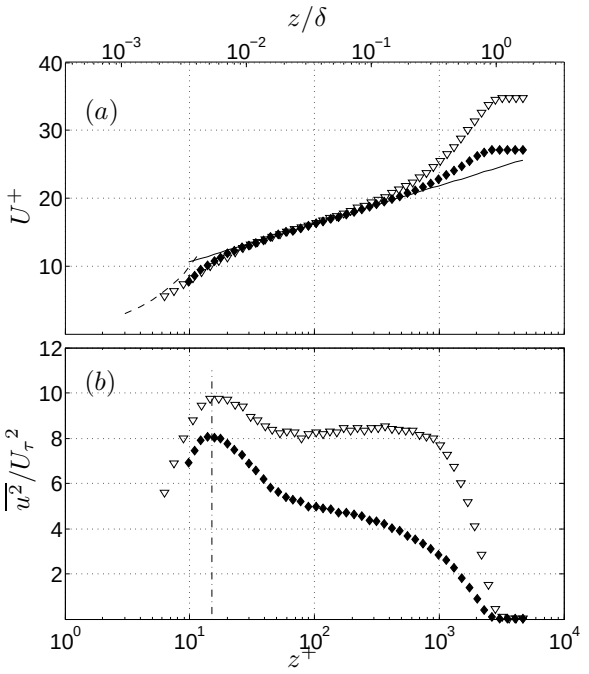


Figure 4: Comparison of APG and ZPG flows at matched $Re_\tau \approx 2800$ (a) Mean velocity profiles (b) Broadband turbulent intensity profiles. (▽) ZPG from HRNBLWT and (⧫) APG. Solid line shows $U^+ = \frac{1}{\kappa}\ln(z^+) + A$, $\kappa$=0.41 and $A$=5.0, dashed line shows $U^+ = y^+$ and dashed-dot line $z^+$=15.

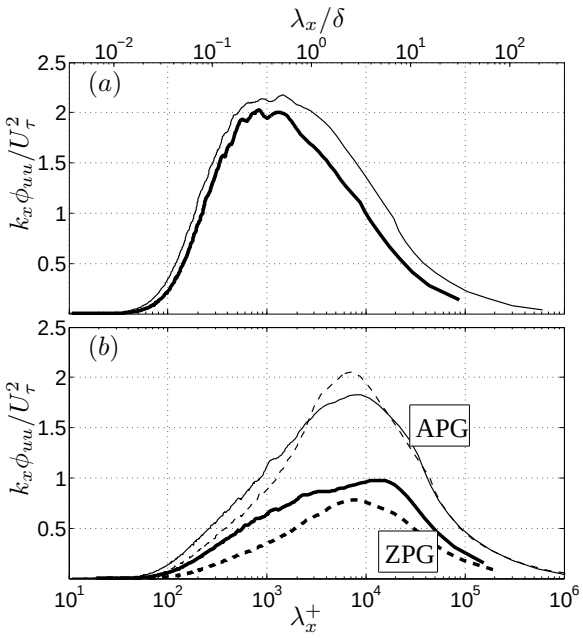


Figure 5: Pre-multiplied energy spectra of streamwise velocity fluctuation $k_x\phi_{uu}/U_\tau^2$ (a) $k_x\phi_{uu}/U_\tau^2$ for the 'inner peak', APG flow (light) and ZPG flow (heavy) at $z^+ \approx 15$ (b) $k_x\phi_{uu}/U_\tau^2$ for APG flow (light) and ZPG flow (heavy), solid-lines for $z \approx (15Re_\tau)^{0.5}$ and dashed-lines for $z/\delta \approx 0.3$.

higher magnitude ($\approx 15\%$) shown in figure 5(a). It can be seen that the higher turbulence intensity $\overline{u^2}/U_\tau^2$ at this wall distance is partly due to increased $\lambda_x^+ = 1000$ energy, but much more due to large scale energy persisting to the wall. Even if another velocity scaling is used to collapse small-scale energy, contribution due to large-scale energy ($\lambda_x > \delta$) would be observed at $z^+ \approx 15$ indicating that, in APG there is even greater influence of superstructure i.e. stronger 'footprint' in the near-wall region.

Figure 5(b) shows that at $z \approx (15Re_\tau)^{0.5}$ (solid line), the energy for APG is twice the level of ZPG, however, peak energy for APG lies at $\lambda_x/\delta = 3$, half of the most energetic wavelength in ZPG. The energy in APG at $\lambda_x/\delta = 6$ is high, however there is more energy at $\lambda_x/\delta = 3$ i.e. $3\delta$ energy dominates but superstructures still exists. Figure 5(b) also shows that at $z/\delta \approx 0.3$ (dashed-line), energy in the APG case is very high. The APG case is more turbulent overall, this can be related to the mean velocity and broadband turbulent intensity profiles in figures 4(a) & (b) where the wake $U^+$ and $\overline{u^2}/U_\tau^2$ are higher in APG than that in ZPG. At this location from the wall, the energy is much lower for ZPG, (approximately 40% of the energy in APG). Despite the huge difference in energy at this location, the peak energy still lies at the same wavelength i.e. $\lambda_x/\delta = 3$ for both flows.

Figures 6(a) & (b) are iso-contour energy maps formed from one dimensional pre-multiplied energy spectra at each wall-normal position. This type of energy spectra map was introduced by Hutchins and Marusic (2007 and 2007b). In these studies (ZPG) it was shown that with high enough $Re_\tau$ (i.e. more than 2000), the energy spectra has two clear energetic peaks. The peak closest to the wall has a location of $\lambda_x^+ = 1000$ and $z^+ = 15$ called the 'inner peak', representing energetic contribution due to the near wall cycle of streaks and quasi-streamwise vortices. The secondary peak occurs in the logarithmic region at $z^+ = (15Re_\tau)^{0.5}$, with a wavelength in outer wall units of $\lambda_x/\delta = 6$, called the 'outer peak'. Figure 6(a) shows the one-dimensional energy spectra for the APG case. While the location of the 'inner peak' is still the same, the 'outer peak' occurs at $z/\delta \approx 0.3$ and at a shorter wavelength of $\lambda_x/\delta = 3$. Figure 6(b) shows the superimposed APG flow energy spectra contour lines onto that of the ZPG. The structure is much different in the logarithmic and wake regions. The most obvious difference in the energy spectra map is that the outer peak occurs at much shorter wave length and the magnitude is much higher. There is much more energy around the $3\delta$ length scale in the outer region.

It is interesting to investigate the structure of the flows at the same Kármán number with varying pressure gradient. We have chosen a few $z$ locations (wall-normal) for comparisons, these are shown in figures 7(a) to (d). In figure 7(a), at $z^+ \approx 15$, energy

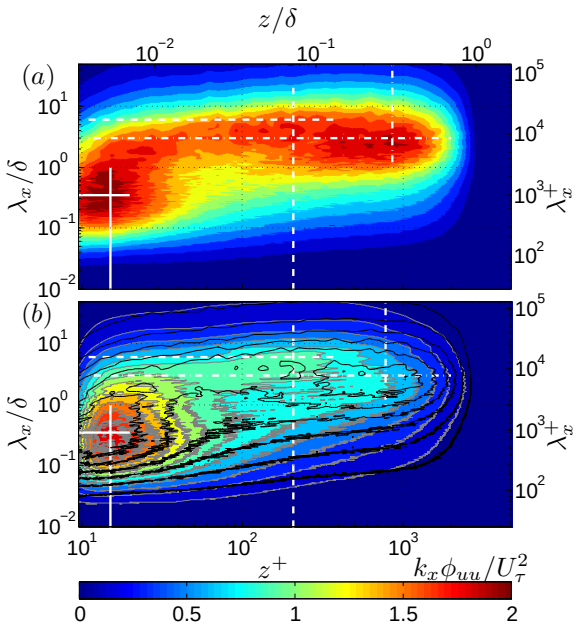


Figure 6: Pre-multiplied energy spectra of streamwise velocity fluctuation $k_x\phi_{uu}/U_\tau^2$. White solid lines indicate $z^+ \approx 15$ and $\lambda_x^+ = 1000$, white dashed line lines indicate $(15Re_\tau)^{0.5}$ and $\lambda_x/\delta = 6$, white dashed-dot lines indicate $z/\delta = 0.3$ and $\lambda_x/\delta = 3$ (a) APG flow at $Re_\tau$ = 2890 ($\triangledown$). (b) Superimposed APG flow energy spectra contour lines onto ZPG at $Re_\tau$ = 2820 ($\blacklozenge$).

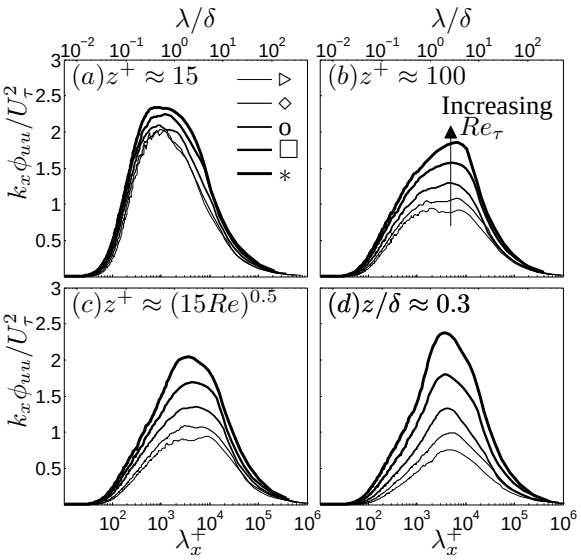


Figure 7: Pre-multiplied energy spectra of streamwise velocity fluctuation $k_x\phi_{uu}/U_\tau^2$ constant $Re_\tau \approx$1800 at selected heights from the wall. $\beta$ increases with line in increasing thickness.

$k_x\phi_{uu}/U_\tau^2$ increases from the condition of ZPG towards strong APG. The center for 'inner peak' is still at $\lambda_x^+ \approx$1000 for all matched $Re_\tau$ data. The presence of large-scale structures can be felt more strongly as $\beta$ is increased.

In figure 7(b) at $z^+ \approx 100$, the energy spectra $k_x\phi_{uu}/U_\tau^2$ reduces for all flows. As $\beta$ increases, the structures with high energy have become more concentrated at $\lambda/\delta \approx$3. At low $Re_\tau$, $k_x\phi_{uu}/U_\tau^2$ has a shape of a plateau, showing that the energy contributions are about balanced from small and large-scales. At high $Re_\tau$, small-scale energy diminishes. At $z/\delta \approx$0.1, $k_x\phi_{uu}/U_\tau^2$ concentrates at $\lambda_x/\delta \approx$3.

At $(15Re)^{0.5}$, the peak energy for ZPG flow occurs at $\lambda/\delta \approx$6 where the 'outer peak' occurs for ZPG flow. Figure 7(c) shows the energy spectra $k_x\phi_{uu}/U_\tau^2$ at $(15Re)^{0.5}$. This figure shows that peak energy at wall-normal position $(15Re)^{0.5}$ occurs at smaller wavelengths as $\beta$ increases. The only difference between this figure and figure 7(b) is that the peak energy spectra location occurs at slightly shorter wavelengths of $\lambda_x/\delta \approx$2 (from $\lambda_x/\delta \approx$3). At $z/\delta \approx$0.3, $k_x\phi_{uu}/U_\tau^2$ concentrates at $\lambda_x^+ \approx$2 shown in figure 7(d). The presence of pressure gradient exaggerates the intensity of energy spectra for case ZPG and $\beta$=1, the level of $k_x\phi_{uu}/U_\tau^2$ reduces as compared with the level of $k_x\phi_{uu}/U_\tau^2$ at wall normal position $(15Re)^{0.5}$, however, for case $\beta$=3.3 & 5.1, the level of $k_x\phi_{uu}/U_\tau^2$ increases.

Figures 8(a) to (e) show one-dimensional energy spectra maps for matched $Re_\tau$ data. In these figures, $\beta$ increased from (a) to (e). In figure 8(a), the 'inner peak' occurs at $z^+ \approx 15$ and $\lambda_x^+ \approx$1000 as expected for a ZPG flow case. There is a trend that large-scale structure present in the near-wall region in the sense that the strength of the energy measured in the intensity of red-colour region energy $k_x\phi_{uu}/U_\tau^2$ is elongated upward as pressure gradient parameter increased to $\beta$=0.87 (figure 8(b)) until $\beta$=5.10 (figure 8(e)). The distribution of energy can be seen more easily in the energy spectra map. Starting with the first data where $\beta$=0 (ZPG), there is no clear outer peak that can be observed in the figure 8(a) as discussed. As $\beta$ increases to 0.87, the 'outer peak' is seen at $\lambda_x/\delta$=5 and $z/\delta$=0.08 seen in figure 8(b). In figure 8(c), $\beta$=1.89, 'outer peak' is observed to present more obviously at $\lambda_x/\delta$=2.5 and $z/\delta$=0.15. In figure 8(d), $\beta$=3.32, 'outer peak' is observed to present at $\lambda_x/\delta$=2 and 0.15$< z/\delta <$=0.4. Finally, in figure 8(e), $\beta$=5.10, 'outer peak' is observed to present at $\lambda_x/\delta$=2 and 0.2$< z/\delta <$0.4.

The behaviour has been observed when we made the comparison at higher $Re_\tau \approx$ 2800 with $\beta$=3.83 in figures 6. We conclude that, the presence of 'outer peak' is dependent on pressure gradient at the same Reynolds number. From a ZPG flow to increasing APG flows, 'outer peak' occurs at $\lambda_x/\delta$=6 and $z/\delta$=0.06 in ZPG flow towards shorter wave length at $\lambda_x/\delta$=2 and further away from the wall at 0.2$<$ $z/\delta <$0.4 in the strongest pressure gradient of our ex-

periment range.

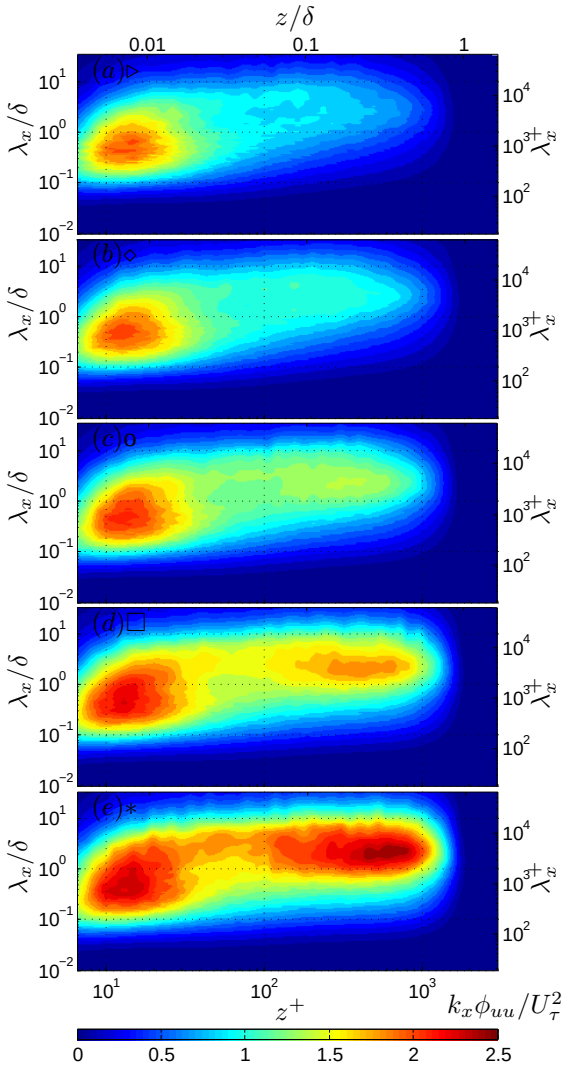


Figure 8: Pre-multiplied energy spectra of streamwise velocity fluctuation $k_x\phi_{uu}/U_\tau^2$ for constant $Re_\tau \approx 1800$. From ZPG case (a) ($\beta$)=0 to (e) $\beta$ =5.1. For detail, refer to Table 1.

## 3 Conclusions

A parametric study in flows starting with ZPG towards APG where the pressure gradient parameter $\beta$ is varied has been conducted. We have summarized the main features in this study as follows. At a constant $Re_\tau$, $\overline{u^2}/{U_\tau}^2$ increases with an increasing pressure gradient. Hutchins et al (2009) established an empirical relationship of $\overline{u^2}/{U_\tau}^2$ as a function of two competing component $l^+$ and $Re_\tau$ in the near wall region. This analysis provides an extension to the above i.e. $\beta$ shall be another parameter where APG flows are considered.

The energy spectra analysis reveals that the presence of an 'outer peak' depends on pressure gradient at the same Reynolds number. This also shall extend the analysis by Hutchins and Marusic (2007, 2007b) where, in the absence of spatial resolution issues, $Re_\tau$ is the only factor to observe an 'outer peak'. For the flow exposed to the biggest pressure gradient of $\beta$=5.10, an 'outer peak' occurs at much shorter length scale of $\lambda/\delta$=2 ($\lambda/\delta$=6 for ZPG) and at a location further away from from the wall $z/\delta$=0.3 ($z/\delta$=0.06 for ZPG). The shifts of these locations are gradual as the strength of APG changes.

## References


Chauhan K.A. Ng, H and Marusic, I. Analysis of oil film interferograms for wall-shear stress measurements using Hilbert-Huang transform, *under consideration in Meas. Sci. Tech*.

Clauser, F.H. (1954), Turbulent boundary layer in adverse pressure gradient, *J. Aero. Sci.*, Vol. 21, pp. 91-108.

Hutchins, N. and Marusic, I. (2007), Evidence of very long meandering features in the logarithmic region of turbulent boundary layers, *J. Fluid Mech.*, Vol. 579, pp. 1-28.

Hutchins, N. and Marusic, I. (2007b), Large-scale influences in near-wall turbulence, *Phil. Trans. R. Soc.*, Vol. 365, pp. 647-664.

Hutchins, N. Nickels, T.B. and Marusic, I. and Chong, M.S. (2009), Hot-wire spatial resolution issues in wall-bounded turbulence, *J. Fluid Mech.*, Vol. 635, pp. 103-136.

Lee, J.H. Sung H.J. (2009), Structures in turbulent boundary layers subjected to adverse pressure gradients, *J. Fluid Mech.*, Vol. 639, pp. 101-131.

Ligrani, P.M. and Bradshaw, P. (1987), Spatial resolution and measurement of turbulence in the viscous sublayer using subminiature hot-wire probes, *Experiments in Fluids*, Vol. 5, pp. 407-417.

Jones, M.B. and Marusic, I. (2001), Evolution and structure of sink flow turbulent boundary layer, *J. Fluid Mech.*, Vol. 428, pp. 1-27.

Kline, S.J. Reynolds, W.C. Schraub, F.A. and Runstadler, P.W. (1967), The structure of turbulent boundary layers, *J. Fluid Mech.*, Vol. 30, pp. 741-773.

Monty, J.P. Hutchins, N. Ng, H.C.H. Chong, M.S. (2009), A Comparison of Turbulent Pipe, Channel and Boundary Layer Flows, *J. Fluid Mech.*, Vol. 632, pp. 431-442.

Nagib, H.M. and Chauhan K.A. (2008), Variation in von Kármán coefficient in canonical flows, *Phys. Fluids*, Vol. 20, pp. 101518:1-10.